JCTC Journal of Chemical Theory and Computation

Article

pubs.acs.org/JCTC

Vibrationally Resolved Absorption and Emission Spectra of Dithiophene in the Gas Phase and in Solution by First-Principle Quantum Mechanical Calculations

E. Stendardo,[†] F. Avila Ferrer,[‡] F. Santoro,*[,‡] and R. Improta*[,†]

[†]CNR−Consiglio Nazionale delle Ricerche, Istituto di Biostrutture e Biommagini (IBB-CNR), Via Mezzocannone 16, I-80136, Napoli, Italy

[‡]CNR−Consiglio Nazionale delle Ricerche, Istituto di Chimica dei Composti Organo-Metallici (ICCOM-CNR), UOS di Pisa, Area della Ricerca, via G. Moruzzi 1, I-56124 Pisa, Italy

Supporting Information

ABSTRACT: The absorption and emission spectra of dithiophene have been computed in different environments (gas phase, apolar, and polar solvents) and at different temperatures, including Duschinsky, temperature and solvent effects at full ab initio level, and considering the anharmonicity of the double well potential associated with the inter-ring torsional mode. The computed spectra are in very good agreement with the experimental ones, allowing for a complete assignment of the main vibrational features. Five different density functionals (BLYP, B3LYP, CAM-B3LYP, BHLYP, and PBE0) have been tested, and CAM-B3LYP and PBE0 are the most accurate.

1. INTRODUCTION

Polythiophenes have attracted considerable interest for their use and their potentialities in several applications in organic electronics, solar cells, and nonlinear optics.[1−3] A deeper understanding of the factors modulating their optical properties and the shape of their absorption and emission spectra is critical for interpreting the available experimental results,[4−12] especially those concerning more complex supramolecular systems,[13] and for designing new materials with purposely tailored properties. In this respect, oligothiophenes have been extensively studied as model for polythiophenes, and they have also been used in several electronic devices.[2,3] Several interesting papers have been devoted to the computation of vibrationally resolved optical spectra of oligothiophenes, providing very useful information on the chemical-physical effects ruling the observed line shape.[14−24] On the other hand, most of the approaches applied up to now[14−18,22] rely on the use of some empirical parameters (e.g., to include the effect of the temperature on the spectra) and/or neglect the Duschinsky effect. Besides decreasing the accuracy of the computed spectra, these limitations can sometimes prevent a quantitative assignment of the experimental spectra. Just to make an example, in the following we show that without including the Duschinsky effect and considering the frequency shifts associated with the electronic transition (i.e., that normal modes and frequencies in the ground and in the excited state can be different), it is not possible to firmly assign the vibrational modes contributing to the different peaks of the low-temperature excitation spectrum of oligothiophenes.[6,12] We have therefore re-examined the optical spectra in solution of oligo-thiophenes, exploiting recent advances in the calculation of vibrational spectra by time-independent methods[44−54] and in the inclusion of solvent effects by continuum models, as the Polarizable Continuum Model (PCM). The cornerstones of our approach will be as follows: (i) complete characterization of the excited state minima and vibrational frequencies at the TD-DFT level, (ii) inclusion of the Duschinsky effect, (iii) nonempirical treatment of temperature effects, (iv) accurate treatment of the effect of the changes in the molecular planarity associated with the electronic transition, (v) inclusion of solvent effect not only on the transition energies but also on the ground and excited equilibrium geometries and normal modes. As a first step we here report a thorough study of the absorption and emission spectra of dithiophene (T2, see Figure 1) in different environments (gas phase, apolar solvent, polar solvent) and at different temperatures. The computed spectra are in very

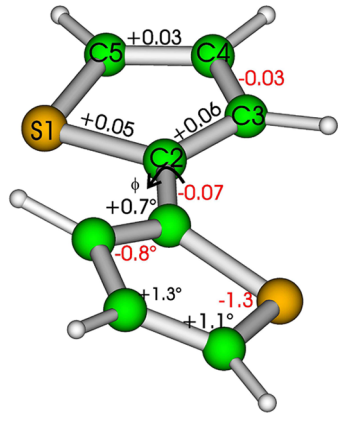

Figure 1. Schematic drawing and atom labeling of dithiophene. The variation in the bond lengths and in the bond angles associated with the $S_0 \rightarrow S_1$ electronic transition (CAM-B3LYP/6-31G(d) calculations) is also shown.

Received: July 30, 2012
Published: October 8, 2012

good agreement with the experimental ones, allowing for a complete assignment of the main vibrational features. For what concerns the electronic methods, this study will also give the opportunity of testing the accuracy of different density functionals (BLYP, B3LYP, CAM-B3LYP, BHLYP, and PBE0) in predicting the vibrational structure of the optical spectra.

This paper is organized as it follows. After discussing the details of our vibronic calculations (Section 2), the first two sections (3.1 and 3.2) of the Results are devoted to the comparison between the performances of the different functionals/basis sets. The assignment of the high-resolution absorption and emission spectra is then performed in Section 3.3, while solvent effects are discussed in Section 3.4. Section 3.5, finally, is devoted to a detailed discussion of the double well existing on the lowest energy torsional mode on S_0 and of the consequent temperature effect on the spectra. Our concluding remarks are reported in Section 4.

2. COMPUTATIONAL DETAILS

2.1. Electronic Calculations. DFT calculations have been employed to compute ground state minima and vibrational frequencies, whereas for the S_1 excited state we resorted to Time-Dependent (TD) DFT calculations, for which analytic gradients are available,[26] followed by numerical calculation of the Hessian. We have compared the performances of 5 different density functionals, namely the gradient corrected BLYP functional,[27,28] hybrid functionals with different ratio of HF exchange, i.e. B3LYP (20% of HF exchange),[29,28] PBE0 (25% of HF exchange),[30] and BHLYP (50% of HF exchange)[31] and the long-range corrected CAM-B3LYP functional.[32] In our calculations we have used five different basis sets, namely the minimal 6-31G(d) and more extended 6-31+G(d,p) and 6-311+G(2d,2p) standard bases and two large Dunning's correlation consistent basis sets augmented with diffuse functions aug-cc-PVTZ and aug-cc-PVQZ.

Bulk solvent effects have been included by the PCM model,[33] resorting to the standard implementation of PCM/TD-DFT, based on the Linear Response theory (LR-PCM/TD-DFT),[34] for which analytical gradient are available, for excited state geometry optimizations[35] and normal modes calculations, while transition energies have been computed also at the State-Specific (SS-PCM/TD-DFT) level.[36−38] Excited state geometry optimizations have been performed in the nonequilibrium (neq) time regime, in order to avoid the overestimation of the transition intensity typical of LR-PCM calculations in the equilibrium time-regime (eq).[36] In any case, we have performed some test excited state geometry optimizations in hexane and dioxane; also at the the solvent eq level. The S_1 frequencies differ by less than 1 cm^{-1} from that obtained at the neq level, indicating that our results are not effected by the choice of the time-regime used in the geometry optimizations. In equilibrium PCM calculations the 'static' dielectric constants at room temperature have been used: namely 1.88 for hexane, 2.20 for dioxane, and 37.21 for dimethylformamide. In nonequilibrium calculations the dielectric constants at optical frequency ($\epsilon_{opt} = n^2$, n is the refraction index) have been used, namely 1.89 for hexane, 2.02 for dioxane, and 2.04 for dimethylformamide. The effect of the temperature on the dielectric constants has not been considered.[18]

All the calculations have been performed by using the Guassian09 package.[39]

2.2. Calculation of the Vibronic Spectra. Due to the brightness of the $S_0 \leftrightarrow S_1$ transition, Franck−Condon (FC) approximation is adequate to the computation of the vibrational structure associated with the absorption and emission spectra. To perform such computations it was necessary to build up a model of the S_0 and S_1 PES. As a starting point we defined harmonic Potential Energy Surfaces (PES) for S_0 and S_1, allowing for Duschinsky rotation of normal coordinates and adopting the so-called Adiabatic Hessian (AH) scheme.[40,41] To that end we located S_0 and S_1 minima and computed the set of normal coordinates $\mathbf{Q}^{(i)}$ and frequencies $\mathbf{\Omega}^{(i)}$ for both the states (i = 0,1 for S_0 and S_1 respectively). The Duschinsky relation holds

$$\mathbf{Q}^{(0)} = \mathbf{J}\mathbf{Q}^{(1)} + \mathbf{K} \tag{1}$$

where $\mathbf{J}$ is the rotation matrix, and $\mathbf{K}$ is the vector of the displacements of equilibrium positions along modes $\mathbf{Q}^{(0)}$.

The S_0 surface shows marked anharmonicity along the central CC bond torsion ϕ. Therefore for S_0 we characterized both the global nonplanar minimum and a low-energy transition state at planar configurations, computing their structures and Hessians. The planar stationary point exhibits an imaginary frequency along the $Q_1^{(0)}$ mode corresponding to a motion along ϕ, and, to reliably describe temperature effects in absorption and emission, it is necessary to undergo an anharmonic description of the ϕ vibrational states. Hazra and Nooijen proposed a computational scheme to deal with double-well profiles, based on the calculation of a one-dimensional (1D) profile of the PES along the imaginary-frequency mode.[42] This method is attractive inasmuch it can describe Duschinsky mixings of the imaginary frequency mode with the other modes, through the usage of an "intermediate" harmonic basis set. Unfortunately, a rigid scan along $Q_1^{(0)}$ Cartesian normal mode leads to an almost vanishing nonplanar minimum (more stable than the planar stationary point by ≈2 cm^{-1}, while the true global minimum is ∼70 cm^{-1} more stable, see below) that does not support any vibrational state. To properly describe the nonplanar minimum is therefore necessary to move to an internal coordinate description and express the torsional states with a suitable basis set. This treatment is much more affordable if the Duschinsky matrix J assumes a block-diagonal form and the dimension of the block of the modes including the imaginary-frequency mode is small (e.g., 2 or 3). We defined a first square-block "A" by starting from $Q_1^{(0)}$ and individuating iteratively all the modes $Q_1^{(0)}$ and $Q_j^{(1)}$ in order that all the S_0 (S_1) modes in the block are projected on the S_1 (S_0) modes by more than 1-ϵ, where ϵ is a convenient small number. Block "B" contains the remaining modes. Strict block-diagonalization is then obtained by setting $J_{ij} = 0$ if $i \in A$ and $j \in B$ or vice versa, and the Duschinsky matrices of each block $\mathbf{J}_C$ are reorthogonalized according to Löwdin $\mathbf{J}_C = \mathbf{J}_C\,(\mathbf{J}_C^T\mathbf{J}_C)^{-1/2}$ with C = A,B.

Once $\mathbf{J}$ is in block-diagonal form, the FC spectrum line shape of the molecule $\sigma(\omega,T)$ at temperature T can be simply computed as a convolution of the two line shapes $\sigma_A(\omega,T)$ and $\sigma_B(\omega,T)$[43]

$$\sigma_C(\omega, T) = \sum_i \sum_f \rho_i \mathbf{FC}_C(i,f)^2 g(\omega - \omega_{fi}, \gamma) \tag{2}$$

$$\sigma(\omega, T) = \int \sigma_A(\omega - \omega', T)\sigma_B(\omega', T)d\omega' \tag{3}$$

$$S(\omega) = C\omega^k\sigma(\omega, T) \quad (4)$$

where i and f are the initial and final vibrational states, ω_{fi} is their energy difference, ρ_i is the thermal population of state i, and $g(\omega,\gamma)$ is a normalized line shape (in the following we adopt a Gaussian) with a width γ. A spectrum $S(\omega)$ directly comparable with experiments (if reported in the frequency domain) can be obtained from eq 4 setting k = 1,3 for absorption and emission respectively, and giving to constant C the proper value to get the spectrum in suitable units (for example the absorption spectrum in terms of molar extinction coefficient $\epsilon(\omega)$).[40,44]

We anticipate that we were able to define a block of dimension 1 (1D) including only the imaginary frequency mode $Q_1^{(0)}$. For future convenience we label this block anharmonic "anh" and harmonic "har" the remaining (3N-7)D block. To describe the ϕ torsional states with a curvilinear coordinate we simply identified $Q_1^{(0)}$ with ϕ for very small displacements and assumed that the coupling of ϕ with the 3N-7 harmonic modes remain vanishing (as it is at ϕ = 0) in all the relevant region of ϕ. Therefore we computed the S_0 and S_1 1D energy profiles along ϕ through a rigid scan from ϕ = 0° to ϕ = 180° with steps of 1 degree at the CAM-B3LYP/6-31G(d) level of theory in the gas phase. The 3N-7 remaining degrees of freedom were frozen at the values they have in the planar stationary point. This approximation, that might be rather crude to investigate the details of very high-resolution spectra, is considered acceptable for the description of broadening effects in room-temperature spectra. The 1D profiles were fitted to the following cosine expansion

$$V^i(\phi) = \sum_{p=0,P} \frac{V_p^i}{2}(1 - \cos p\phi) \quad (5)$$

where i = 0,1 identifies the ground or excited PES, respectively. The 1D Hamiltonian was expressed as

$$H^i(\phi) = -B_0\frac{d^2}{d\phi^2} + V^i(\phi) \quad (6)$$

where B_0 is the internal rotation constant $B_0 = \hbar^2/(2I_{rid})$ and the reduced moment of inertia I_{rid} was computed as $I_{rid} = I_1I_2/(I_1 + I_2)$, and where I_1 and I_2 are the moments of inertia with respect to the central bond axis of the two halves of the molecule bridged by the central bond.

Anharmonic eigenfunctions $|\phi^i\rangle$ were computed by solving the secular equation $\mathbf{H}^i\mathbf{C}^i = \mathbf{C}^i\mathbf{E}^i$ on a basis of sines and cosines $1/(2\pi)^{1/2}$, $(\cos n\phi/\sqrt{\pi},..n = 1, N_{max})$, $(\sin n\phi/\sqrt{\pi},..n = 1, N_{max})$; the 1D FC overlaps $\mathbf{FC}_{anh}^{i\to j}$ were obtained by projecting the $|\phi^j\rangle$ eigenstates onto the $|\phi^i\rangle$ ones $\mathbf{FC}_{anh}^{i\to j} = (\mathbf{C}^i)^T\mathbf{C}^j$. This approach is analogous to what was already employed for the torsional degree of dithiophene in ref 55. The absorption and emission line shape for torsion at 300 K was also approximated by adopting a classical analogue of the Franck−Condon principle. In this case (i) we computed the classical probability density for ϕ as $P^i(\phi,T) = Z^{-1}exp[-V^i(\phi)/k_BT]$ where Z is the relevant partition function and k_B is the temperature, (ii) we generated a random sequence of numbers distributed according to $P^i(\phi,T)$ (technically we first fitted $P^i(\phi,T)$ with a combination of Gaussian functions and then adopted standard routines to generate a random sequence of numbers with a Gaussian distribution), (iii) for each member of the sequence we computed the energy difference $V^1(\phi) - V^0(\phi)$ and collected them into bins, forming a histogram, and, finally, (iv) we fitted the histogram with an analytical function to obtain a smooth line shape (we adopted a biexponential which provides very accurate fits; the accuracy deteriorates remarkably by adopting a monoexponential).

The relevant FC overlaps of the *har* block were obtained by standard recurrence formulas[45,46] and an effective preselection scheme developed in our group[47−53] and implemented in the freely available code *FCclasses*.[54] This approach is somewhat similar to what was done already reported by Heimel et al. for oligo-(para-phenylenes),[25] where however, Duschinsky effects in the (3N-7)D block were neglected ($\mathbf{J}$ = **1** in eq 1) and technically the eigenstates of the torsional Hamiltonian in eq 6 were computed on a discrete grid of points (and not expanded on a basis set), and by Borrelli and Peluso for ethylene,[56] expressing all the 3N-6 normal coordinates in terms of internal coordinates (see also ref 57) and adopting a finite Fourier series (equivalent to our sine and cosine series) to expand the torsional eigenstates.

3. RESULTS

3.1. Dithiophene in the Gas Phase. We have optimized the geometry of T2 in the gas phase by using different functionals (PBE0, CAM-B3LYP, BHLYP) and different basis sets (see Tables 1 and 1 in the SI). Confirming previous analysis (see ref 58 and references therein) all the density functionals predict that the absolute minimum is not planar, with the two thiophene rings forming a dihedral angle of ∼25° (see Figure 1). This estimate is close to that computed in previous studies and to the experimental estimate (∼21°).[6] In any case, the energy barrier associated with the ϕ variation in the gas phase is small, and accordingly the energy profile is very flat as indicated by the low-frequency associated with ϕ torsion. Its CAM-B3LYP/6-311+G(2d,2p) estimate in the nonplanar minimum level is 35 cm^{-1}, but it is rather insensitive to the level of the computation, fully consistent with the experimental

Table 1. Lowest Energy Vertical Absorption (ν_A) and Emission (ν_E) Energies (in eV) Computed for T2 in the Gas Phase by Using Different Functionals and Basis Sets[b]

TD	I	II	III
	CAM-B3LYP		
ν_A	4.50(0.41)	4.34(0.39)	4.30(0.37)
$\nu_A{}^a$	4.35(0.42)**3.88**	4.18(0.41)	4.13(0.38)
ν_E	3.60(0.43)	3.44(0.42)	3.39(0.39)
	PBE0		
ν_A	4.26(0.42)	4.11(0.41)	4.07(0.38)
$\nu_A{}^a$	4.16(0.44)**3.77**	4.00(0.44)	3.95(0.39)
ν_E	3.58(0.44)	3.42(0.43)	3.37(0.40)
	BHLYP		
ν_A	4.55(0.42)	4.39(0.40)	4.34(0.37)
$\nu_A{}^a$	4.40(0.43)**3.90**	4.22(0.41)	4.17(0.38)
ν_E	3.62(0.44)	3.45(0.43)	3.40(0.40)
	B3LYP		
$\nu_A{}^a$	4.03(0.42) **3.64**	3.86(0.42)	3.82(0.38)
	BLYP		
$\nu_A{}^a$	3.72(0.41) **3.40**	3.55(0.41)	3.67(0.56)

[a]Planar minimum. Basis sets: I = 6-31G(d); II = 6-31+G(d,p); III = 6-311+G(2d,2p); Exp. 0−0 jet expansion 3.86 eV. (*J. Phys. Chem.* **1994**, *98*, 12893) CASPT2 results: 3.99−4.1 eV.[6] [b]Oscillator strengths are given in parentheses, 0-0 transition energies are given in bold.

value measured in jet-cooled conditions (25 cm^{-1}),[6] considering the error due to the use of the harmonic approximation.

It has indeed been suggested that, when embedded in a organic glass at very low temperature, T2 is planar already in the S_0 minimum.[22,59] Our analysis of the temperature dependence of the spectra, reported in the following sections, supports this hypothesis, though it is reasonable to assume that the shape of the PES along ϕ is much shallower than in S_1.

Therefore we have also optimized S_0 under planarity constraint, and, whenever not otherwise specified, the spectra have been computed modeling the S_0 PES as a quadratic with minimum at the S_0 planar minimum. This latter is very close in energy to the absolute minimum (the energy difference being <100 cm^{-1}) and features only one very low imaginary frequency (see Table 1 in the SI).

The most significant geometry shifts associated with the $S_0 \rightarrow S_1$ (corresponding to a HOMO→LUMO excitation) electronic transition are given in Figure 1. In line with the bonding/antibonding character of the molecular orbitals (MOs) involved in the transition, they involve the decrease of the C2C2′ bond distance (suggesting a partial double-bond character on S_1) and the increase of the C2C3 and C2′C3 bond lengths. As already discussed, in S_1 minimum T2 adopts a planar geometry with a larger frequency than in S_0 (73 cm^{-1} according to CAM-B3LYP/6-311+G(2d,2p) calculations), associated with the rotation around ϕ, in line with the partial double-bond character of the C2C2′ bond.

3.2. Optical Spectra in the Gas Phase: The Effect of the Functional. As a first step we have computed the vertical excitation (ν_A, from the S_0 minimum) and emission (ν_E, from the S_1 minimum) energies for T2 in the gas phase, by using 5 different functionals. The results obtained by using three different basis sets on the 6-31G(d) optimized geometry are reported in Table 1, while Figure 2 shows the spectra computed

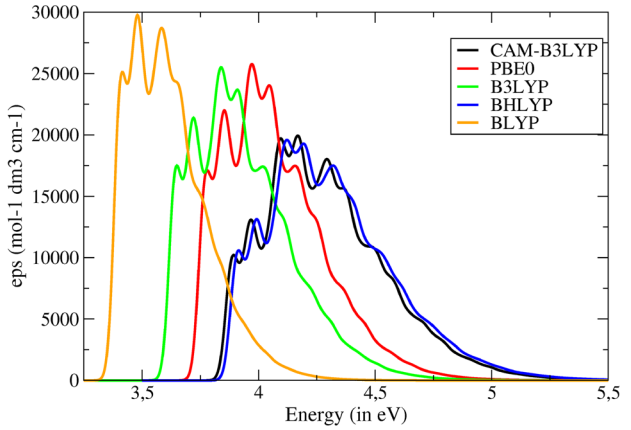

Figure 2. Absorption spectra computed in the gas phase for T2 at 0 K by using 5 different functionals and the 6-31G(d) basis set, convoluting each transition by a Gaussian with HWHM 0.03 eV.

at the 6-31G(d) level. All the examined functionals predict qualitatively similar absorption spectra (a detailed analysis of the line shape is postponed to the next sections), but significant quantitative differences are found. ν_A roughly increases with the amount of HF exchange included in the functional: a pure functional as BLYP predicts that ν_A is ∼0.8 eV red-shifted with respect BHLYP functionals, including 50% of HF exchange. As it could be expected, ν_A in the absolute minimum is noticeably larger (by ∼0.10−0.15 eV) than that computed in the planar minimum.

Comparison between ν_A and the experimental absorption spectrum is not straightforward.[40] The maximum of the absorption band is significantly red-shifted with respect to the computed ν_A, also due to the smaller (∼0.1 eV) zero-point vibrational energies of S_1. Vapor phase spectra shows a broad band centered around 4.2 eV,[7] but the comparison between spectra computed at 0 K with room-temperature experiments is made more difficult by large temperature effects on the absorption spectrum (see the section below). However, supersonic-jet experiments indicate that the 0−0 transition energy is ∼3.86 eV, suggesting that BLYP significantly underestimates ν_A. B3LYP ν_A is also too low, especially when considering that the computed ν_A decreases when the size of the basis set increases. Oscillator strength is overestimated by 30% with respect to the experimental value (0.29) by all the density functionals.

On the balance the most accurate results are obtained by BHLYP (confirming its accuracy in the calculation of vibrationally resolved spectra),[60] PBE0, and CAM-B3LYP. In the following our analysis will be mainly based on these two latter functionals, whose reliability is also supported by extensive statistical studies on the performances of different functionals in the computation of optical spectra,[61] concerning also the calculation of the 0−0 transition energies,[62] and the simulation of the optical line shape in anthraquinone derivatives[63] and phenylacetylene.[64]

The line shape of the spectrum does not change significantly with the basis set (see Figure 2 in the SI), but for a small decrease of the absorption intensity, which gets closer to the experimental one. Inspection of Figure 1 and of Table 2 of the SI (where the ν_A computed at the aug-cc-PVQZ//6-31G(d) level are also reported) indicates that the 6-31+G(d,p) results are close to the converged ones.

Before proceeding in our analysis, it is worth noting that our computations predict that the second bright state of dithiophene (S_2) is ∼1.2−1.3 eV higher in energy than S_1: ν_A(S2) is 5.18 eV and 5.54 eV according to TD-PBE0/6-311+G(2d,2p)//PBE0/6-31G(d) and TD-CAM-B3LYP/6-311+G(2d,2p)//CAM-B3LYP/6-31G(d) calculations, respectively, and its oscillator strength with S_0 is ∼ three-times smaller. The S_1−S_3 energy profiles along ϕ at TD-CAM-B3LYP/6-31G(d) level are shown in the SI. Our estimates are in good agreement with the experimental spectra providing a peak at 5.1 eV, whose oscillator strength (0.13) is significantly smaller than that of the $S_0 \rightarrow S_1$ transition.

3.3. High-Resolution Spectra in the Gas Phase: Comparison with the Experiments. Experimental high resolution emission spectra are available for T2 both in jet-cooled beam[6] and in hexane matrix at 4 K,[12] allowing for interesting comparison with our calculations. The former spectrum is not well resolved, but it can can be more directly compared to our gas phase calculations. The latter is more resolved, but, besides being affected also by intermolecular interactions with the glass matrix, it lacks the 0−0 transition. As a consequence, we shall consider both experimental spectra in our analysis. As stated above, the planar S_0 minimum is used for computing the spectra.

In order to qualitatively compare the performances of the different functionals, we start by comparing the stick emission spectra computed at the 6-31G(d) level with the experimental spectra obtained in hexane glass (see Figure 2 in the SI).

Table 2. Comparison with the Main Vibrational Features of the Emission Spectrum of T2, According to Different Computational Approaches, and the Experimental Results[a]

			CAM-B3LYP				
		PBE0	basis set				
band	S_0 mode	I	I	III	III + anharm[c]	exp[a]	exp[b]
A	$\nu_5^{(0)}$	297(0.12)	296(0.16)	296(0.25)	294	298(0.36)	304(0.56)
B	$\nu_6^{(0)}$	384(0.37)	384(0.39)	384(0.49)	381	391(0.45)	382(0.49)
C	$\nu_{12}^{(0)}$	695(0.55)	694(0.50)	697(0.49)	689	682(0.38)	694(0.72)
D	$\nu_{16}^{(0)}$	762(0.18)	759(0.23)	765(0.25)	754	752(0.28)	762(0.38)
E	$\nu_{34}^{(0)}$	1529(0.51)	1543(0.74)	1513(0.72)	1476	1455(0.78)	1469(0.82)
F	$\nu_{36}^{(0)}$	1636(0.26)	1652(0.38)	1628(0.40)	1589	1569(0.55)	1576(0.48)
G		[d]	1835(0.13)	1809(0.25)	1770	1747	
H		1914(0.19)	1927(0.28)	1899(0.34)	1857	1839	
I		2224(0.30)	2237(0.39)	2210(0.37)	2167	2135	

[a]Reference 12. [b]Estimated from ref 6. [c]Frequencies corrected for anharmonicity according to ref 70. [d]More than one contribution. [a]Relative intensities are given in parentheses. A schematic description of the vibrational modes ($\nu_x^{(0)}$, x being the number of the mode in order of increasing frequency) associated with the peaks can be found in the SI.

Confirming the conclusion of our analysis of the absorption spectrum, all the functionals examined qualitatively well reproduce the experimental line shape. The most significant quantitative discrepancies concern the relative height of the different peaks and the overestimation of the energy of the peaks with frequency >1000 cm^{-1} (especially at the BHLYP level), which mainly depends on the small size of the basis set employed (see below). Also in this case, BLYP exhibits the worst performances, since the frequency of the strong feature around 1500 cm^{-1} is underestimated already at the 6-31G(d) level while the intensity of the peak at ~700 cm^{-1} is significantly exaggerated. Actually, the most significant differences between the different functionals concerns the relative height of the features at ~1500 cm^{-1} and that at ~700^{-1}. Some functionals, such as CAM-B3LYP, predict that the former is significantly more intense, whereas others, such as PBE0 and B3LYP, predict that those peaks have similar intensities. On the other hand, the relative height of these features strongly depends on the experimental conditions, as shown by the data of Table 2, where we have reported the frequencies and the relative height with respect to the 0−0 transition of the fluorescence spectrum of jet-cooled T2, estimated on the grounds of Figure 5 of ref 6. While in supersonic-jet the peaks at ~1500 cm^{-1} and at ~700^{-1} have similar intensities, in hexane matrix the former is twice more intense, probably indicating an increase/decrease of the displacement of S_0 and S_1 equilibrium geometries along the former/latter mode. The two sets of 'experimental' frequencies are instead very similar, within the uncertainty inherent to the procedure we have used to estimate the experimental values. On the balance, the computed spectra are very accurate, since all the main features of the experimental spectra are correctly reproduced. The frequencies computed at the 6-31G(d) level are shown to be significantly overestimated. On the other hand, when a larger basis set is used and anharmonic corrections are included, the computed frequencies are close to the experimental ones (without using any scaling factor), the average deviation for the 8 lowest energy main peaks being ~13 cm^{-1} (CAM-B3LYP calculations), as confirmed by Figure 3 where the computed spectra are compared with the experimental one.

On the ground of the good agreement between computed and experimental spectra, we can more confidently proceed to assign the main feature of the experimental spectrum, based on CAM-B3LYP/6-311+G(2d,2p) calculations (see Figure 3 for the labeling of the different peaks and Figure S4 in the SI for a schematic description of the relevant vibrational modes, which are labeled in the order of increasing frequency).

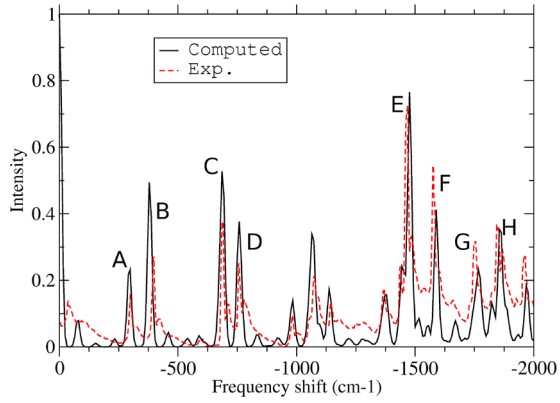

Figure 3. High resolution emission spectrum computed in the gas phase at 0 K for T2 at the CAM-B3LYP/6-311+G(2d,2p) level, including anharmonic corrections on the ground state frequencies and convoluting all the stick transitions with a Gaussian with HMHW = 10 cm^{-1}. The experimental spectrum computed in hexane matrix at 4 K is also shown. The height of the spectra has been normalized by imposing that the feature at ~1500 cm^{-1} has the same intensity of the experimental spectrum.

1. The peak **A** at ~300 cm^{-1} corresponds to the fundamental of S_0 mode $\nu_5^{(0)}$, which can be described as a global breathing mode of T2, leading to variation of the SC2C2′ angles and the SC3′ and S′C3 distances.

2. The peak **B** at ~390 cm^{-1} is the fundamental of S_0 mode $\nu_6^{(0)}$, namely a variation of the C3C2C2′ bond angle.

3. The peak **C** at ~690 cm^{-1} is due to the fundamental transition of S_0 mode $\nu_{12}^{(0)}$, breathing modes of the two rings.

4. The peak **D** at ~760 cm^{-1} is the fundamental of S_0 mode $\nu_{16}^{(0)}$, characterized by strong contributions from C4C3C2 and C4′C3′C2′ bendings.

5. The peak **E** at ~1460 cm^{-1} is the fundamental of S_0 mode $\nu_{34}^{(0)}$ which corresponds to CC double bond stretchings, with main components on C4C5 and C4′C5′ stretchings coupled to the C2C2′ one.

6. The peak **F** at ~1570 cm^{-1} also corresponds to the fundamental of a mode that is a combination of CC double

dx.doi.org/10.1021/ct300664d | J. Chem. Theory Comput. 2012, 8, 4483−4493

Table 3. Description of the Main Vibrational Features of the Absorption Spectrum of T2, According To Different Computational Approaches[c]

		PBE0	CAM-B3LYP				
			solvent and basis set				
band	S_1 mode	GP I	GP I	HEX I	GP III	descr.[b]	exp[a]
a	$\nu_5^{(1)}$	290(0.14)	288(0.15)	290(0.15)	289(0.24)	$\nu_5^{(0)}$ (0.99)	287
b	$\nu_7^{(1)}$	385(0.36)	386(0.36)	386(0.33)	386(0.44)	$\nu_7^{(0)}$ (0.99)	385
c	$\nu_{14}^{(1)}$	672(0.91)	672(0.97)	672(0.97)	673(0.98)	$\nu_{12}^{(0)}$ (0.87)+ $\nu_{15}^{(0)}$ (0.11)	663
d	$\nu_{16}^{(1)}$	715(0.06)	711(0.04)	712(0.04)	713	$\nu_{15}^{(0)}$ (0.87)+$\nu_{12}^{(0)}$(0.11)	692
b+c		1057(0.32)	1058(0.34)	1058(0.32)	1060(0.42)		1047
2c		1343(0.40)	1344(0.45)	1344(0.44)	1347(0.46)		1324
f	$\nu_{36}^{(1)}$	1632(0.81)	1666(1.32)	1671(1.24)	1643(1.14)	$\nu_{36}^{(0)}$ (0.50)+$\nu_{34}^{(0)}$(0.38)	1592
b+f		2017(0.31)	2052(0.45)	2057(0.46)	2030(0.54)		1976

[a]Ref 12. [b]To describe the transitions and correlate absorption and emission bands, for each S_1 modes $\nu_x^{(1)}$ (x being the number of the mode in order of increasing frequency) we indicate the S_0 mode it corresponds, by looking at the largest square elements of the Duschinsky matrix **J** (given in parentheses) that identify the most similar S_0 modes. As an example absorption band **c** is a fundamental of mode $\nu_{14}^{(1)}$, this mode is projected by 0.87 on S_0 mode $\nu_{12}^{(0)}$ and by 0.11 on S_0 mode $\nu_{15}^{(0)}$. The description is relative to GP I results. [c]Frequency in cm^{-1}. Relative intensities are given in parentheses. Basis sets: I 6-31G(d), III (6-311+G(2d,2p). GP = gas phase; HEX = hexane.

bond stretchings ($\nu_{36}^{(0)}$), but in this case C2C2′ stretching is coupled to C3C2 and C3′C2′ bond stretchings.

7. The peaks **G**, **H**, and **I** correspond to combination bands with one quantum on normal mode $\nu_{34}^{(0)}$ and one quantum on modes $\nu_5^{(0)}$, $\nu_6^{(0)}$, and $\nu_{12}^{(0)}$, respectively.

The availability of fluorescence excitation spectra in n-hexane matrix at 4.2 K[12] enables a comparison with the high resolution absorption spectrum and useful insights on the S_1 normal modes (see Table 3 and Figure 4). Also for absorption the main features of the experimental spectrum[12] are well reproduced by our computations. Although inclusion of anharmonic corrections on excited state frequencies is not yet possible (explaining the overestimation of vibrational frequencies >1000 cm^{-1}), the computed frequencies are also in good agreement with the experimental results. The Duschinsky effect cannot be overlooked. Indeed the main peaks of the spectrum (those ruling the absorption spectrum, see below) do not correspond to transitions of pure S_0 modes but to fundamentals of S_1 modes arising from the mixing of two or even three S_0 vibrational modes. As a consequence, while in the emission spectrum we see two strong peaks around 700 cm^{-1} (**C** and **D**) and two around 1500 cm^{-1} (**E** and **F**), in the absorption spectrum there is only one peak around 700 cm^{-1} (**c**) and one around 1500 cm^{-1} (**f**).

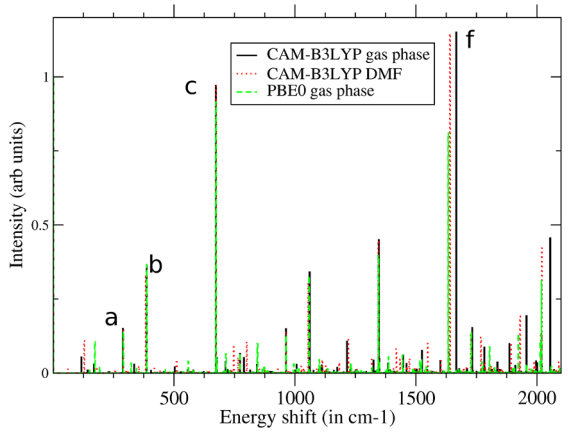

Figure 4. High resolution absorption spectrum computed in the gas phase and in DMF solution at 0 K for T2 by using the 6-31G(d) basis set. The height of the spectra has been normalized by imposing that the 0−0 transition has intensity = 1.

3.4. Optical Spectra in Solution. Experiments indicate that solvent does not have any dramatic effect on the absorption and emission spectra of T2. At room temperature, when going from the gas phase to a nonpolar solvent like hexane the 0−0 transition energy is red-shifted by less than 800 cm^{-1} and the absorption maximum by 1500 cm^{-1}.[7] SS-PCM calculations (see Table 4) do not predict any significant solvent shift. In the planar minimum the dipole moment of the ground and of the excited state is practically zero, and the ν_A computed in DMF is almost coincident to that predicted in the gas phase. In the nonplanar minimum, a very small red-shift (0.01 eV) is predicted in hexane at the SS-PCM/CAM-B3LYP/6-31G(d) level, which does not significantly change using the more extended 6-31+G(d,p) basis set. In any case, it is not surprising that SS-PCM calculations, which are sensitive to the effect

Table 4. Vertical Absorption (ν_A) and Emission (ν_E) Energies (in eV, Osc. Strengths Are Given in Parentheses) and 0-0 Transition Energy of T2 Systems in Different Environments, According to CAM-B3LYP/6-31G(d) Calculations[c]

		hexane		dioxane		DMF	
	gas phase	LR-PCM	SS-PCM	LR-PCM	SS-PCM	LR-PCM	SS-PCM
ν_A	4.50(0.41)	4.40(0.49)	4.49(0.41)	4.39(0.49)	4.49(0.41)	4.36(0.50)	4.46(0.41)
$\nu_A{}^a$	4.35(0.42)	4.26(0.50)	4.35(0.42)	4.25(0.51)	4.35(0.42)	4.24(0.51)	4.34(0.42)
$0-0^{a,b}$	3.96	3.84	3.96	3.83	3.96	3.83	3.95
ν_E	3.60(0.43)	3.46(0.51)	3.58(0.43)	3.45(0.42)	3.58(0.43)	3.45(0.52)	3.57(0.43)

[a]Planar minimum. [b]Without including zero-point energies. SS-PCM/CAM-B3LYP/6-31+G(d,p) calculations in hexane, 4.17 eV, in the gas phase 4.18 eV. [c]Planar minima have been considered for S_0.

associated with the variation of the dipole moment,[36] does not reproduce the observed small red-shift: the dipole moment shift associated with the electronic transition in T2 is very small. For the planar minimum is zero by symmetry, and the very small changes with respect to the gas phase are due to quadrupolar effects. No significant shift is therefore expected in polar solvent (for example when going from hexane to DMF), as confirmed by the experimental results in methanol.[7]

The transition energy could be affected by the polarizability of the embedding medium, and this effect is not expected to be accurately reproduced by standard implementation of a continuum model. Actually in LR-PCM calculations, solvent shift is proportional to the transition intensity,[36,67] and this result can be put in relation with the effect of the change in the molecular polarizability associated with the electronic transition.[67,68] Interestingly, LR-PCM/CAM-B3LYP calculations predict that in hexane ν_A is red-shifted by ~0.1 eV, in line with the experimental results.

The absorption and emission spectra computed in DMF at 0 K are compared with the low temperature experimental spectra in Figure 5. The computed spectra have been shifted in order to match the maximum of the experimental one, and this shift provides an estimate of the absolute error of our calculated transition energies. At the LR-PCM/CAM-B3LYP/6-31+G(d) level, the computed absorption and emission spectra have been red-shifted by 0.065 and 0.075 eV, respectively. At the SS-PCM/CAM-B3LYP/6-31+G(d) level, the shifts are 0.20 eV for both absorption and emission. As a consequence, our calculations reproduce almost quantitatively the experimental Stokes shift. Although LR-PCM results are closer to the experimental ones, it is important to remind that extension of the basis set causes a red-shift by ~0.2 eV of the computed ν_A. If this effect is taken into account, SS-PCM spectra would be almost superimposed to the experimental ones, while the LR-PCM spectra would be ~0.13 eV red-shifted.

The most significant discrepancy between the computed and the experimental spectra concerns the relative intensity of the 0−0 peak in the absorption spectrum, whose intensity is noticeably underestimated by our calculations. This result is likely due to a slight overestimation of the geometry shifts associated with the electronic transition.

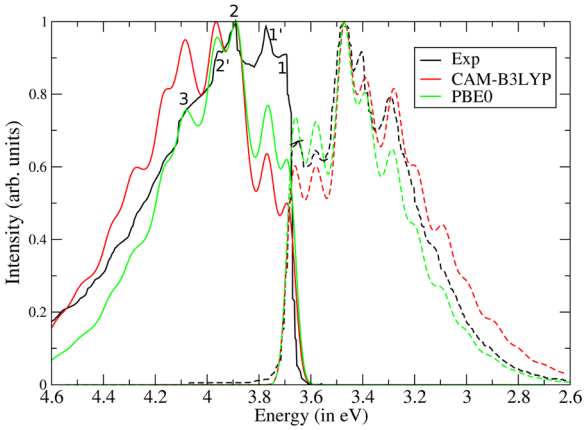

Figure 5. Absorption and emission spectra computed in DMF at 0 K for T2 at the PCM/CAM-B3LYP/6-31G(d) and PCM/PBE0/6-31G(d) levels, convoluting each transition by a Gaussian with HWHM 0.03 eV, compared with the spectra measured in ethanol glass at 77 K.

The analysis of the computed spectra indicate that, besides the 0−0 transition, the lowest energy feature of the absorption spectrum (1 in Figure 5), receives significant contribution from the fundamental of mode $\nu_7^{(1)}$ (**b** peak in Figure 4) and of mode $\nu_7^{(1)}$ (**c** peak). The maximum of the absorption (2 in Figure 5) band is due to the fundamental of mode $\nu_{36}^{(1)}$ (**c** peak in Figure 4 and in Table 3). The close lying shoulder (2′) on the blue-side is due to a combination band with one quantum on modes $\nu_{36}^{(1)}$ and $\nu_{14}^{(1)}$ (**f**+**c**), with a contribution from the (**f**+**b**) transition. Finally, the feature labeled as 3 in Figure 5 is mainly due to the first overtone of transition (**f**).

3.5. Double-Well and Temperature Effects. A reliable simulation of the temperature effects requires a proper treatment of the anharmonic effects along the torsion ϕ. The inset of the upper panel of Figure 6 shows the computed profiles in the gas phase at the CAM-B3LYP/6-31G(d) level of theory, freezing all the other degrees of freedom at the geometry of the planar S_1 minimum (different profiles considering as reference geometry S_0 minimum or the S_1 nonplanar minimum are reported in the SI). The S_0 profile is very flat and shows a double-well shape in the region $\phi = 0°$ of the *trans* isomer. In the same region a single-well with an almost harmonic profile is seen on S_1; at $\phi = 90°$ this latter exhibits a very peaked shape due to an intersection with a higher lying state (see Figure 2 in the SI). The potential energy profiles have been fitted to the cosine expansions in eq 5 including all the $p \leq 10$ (the parameters are given in the SI). For the S_1 profile we did not consider in the fit the points for $70° < \phi < 110°$ and $-110° < \phi < 70°$, since they are not

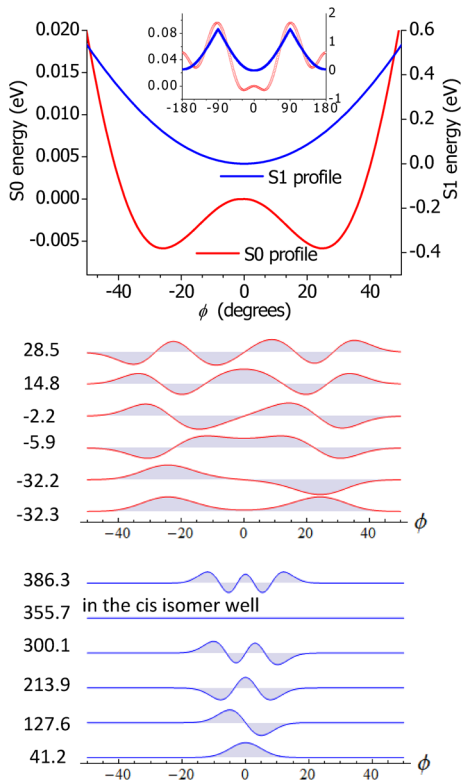

Figure 6. Upper panel: S_0 and S_1 CAM-B3LYP/6-31G(d) energy profiles for a rigid rotation along ϕ starting from the S_0 planar stationary point; S_0 (central panel) and S_1 (lower panel) lowest-energy eigenfunctions along ϕ, labeled by their energy in cm^{-1} with respect to the $\phi = 0°$ energy.

dx.doi.org/10.1021/ct300664d | J. Chem. Theory Comput. 2012, 8, 4483−4493

relevant for the spectra computed here, but their inclusion deteriorates the fit in the region of the bottom of the wells.

On the ground of these fits we computed the energy eigenfunctions of the Hamiltonian in eq 6 for S_0 and S_1. At the S_0 planar stationary point the rotational constant is $B_0 = 0.325$ cm^{-1}; in the vibrational calculations it has been considered independent of the geometry. The reliability of such an estimate of B_0 is supported by the fact that, as discussed in more detail in the following, adopting this value for B_0 and approximating $V^1(\phi)$ around the minimum $\phi = 0°$ as a quadratic function one gets a harmonic frequency very close to what was computed by Gaussian 09 in Cartesian coordinates. The central and lower panels of Figure 6 report respectively the lowest six S_0 and S_1 eigenfunctions, plotted in the region $-50° < \phi < 50°$ and labeled with their energies in wavenumbers with respect to the PES energy at $\phi = 0°$; the upper panel gives the S_0 and S_1 profiles in the same ϕ range. It is seen that the S_1 states closely resemble harmonic states with an effective frequency of ≈85 cm^{-1}, which nicely agree with the 84.24 cm^{-1} value computed by Gaussian09 in Cartesian coordinates. At variance, the S_0 states show strong anharmonicities, and, as expected for a double-well profile, they are grouped in pairs of symmetric and antisymmetric states with an energy-splitting increasing with energy. The lowest states, below the barrier, are combinations of states localized in the wells, their probability density being maximum at $\phi \approx \pm 25°$ and vanishing at $\phi = 0°$; this feature has a strong impact on the spectra profile. In fact, the central panel of Figure 7 documents that absorption and emission line shapes along ϕ are drastically different, being the former much broader than the latter. Stick spectra have been convoluted with a Gaussian with HWHM = 0.005 eV, and the gap between the S_1 and S_0 energies at $\phi = 0°$ was set to zero.

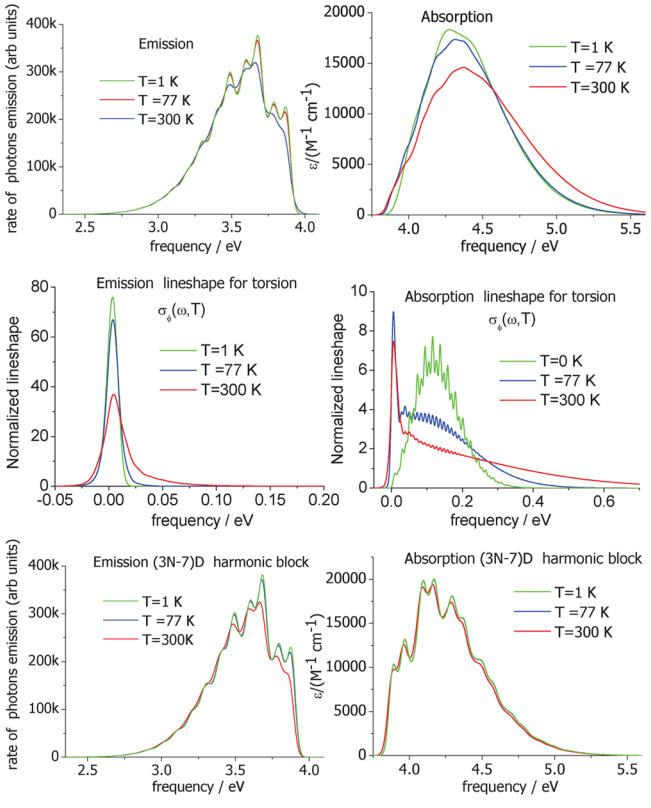

Figure 7. CAM-B3LYP/6-31G(d) emission and absorption spectra for the (3N-7)D block (lower panels), the 1D ϕ anharmonic block (central panels) and the complete T2 molecule (upper panels) at T = 1, 77, and 300 K. As explained in the text the latter can be considered convoluted with a Gaussian with HWHM = 0.03 eV.

Already at T = 1 K absorption manifests a very long vibrational progression. The reason for that can be understood inspecting the eigenfunctions in Figure 6: because of the localization in the nonplanar wells, the lowest-energy S_0 states do not overlap significantly with the lowest-energy S_1 states; on the contrary they overlap with S_1 that extend in the region $\phi \approx \pm 25°$ and therefore are characterized by a large number of quanta. At the increase of the temperature S_0 states above the barrier are populated too, with a maximum of probability density at $\phi \approx 0°$; because of that they remarkably overlap with the lowest S_1 states, explaining the rise of a peak in the absorption spectrum at approximately zero frequency.

The lower panels in Figure 7 report the spectra of the (3N-7)D harmonic block. To separate this block from mode Q_1 (associated with ϕ) we resorted to the block-diagonalization procedure outlined in Section 2.2, adopting a threshold $1\text{-}\epsilon$ = 0.925, which guarantees that the neglected Duschinsky couplings are weak. The spectra have been obtained convoluting the stick spectra with a Gaussian with HWHM = 0.02958 eV. Fully converged spectra at finite temperature for the harmonic block have been obtained by the prescreening method presented in ref 43. The temperature dependence is rather weak but, at variance with what happen for the anharmonic block, slightly more pronounced in emission than in absorption. The upper panels in Figure 7 give the spectra of the whole molecule obtained through convolution of the blocks' spectra according to eq 4. Due to the fact that the convolution of two gaussians is still a Gaussian with a variance equal to the sum of the two, this spectrum is equivalent to what would have been obtained convoluting the stick spectra of the full-dimensionality (3N-6)D system with a Gaussian with HWHM = 0.03 eV. Emission spectrum strongly resembles the one of the (3N-7)D block and inclusion of ϕ spectrum only slightly broaden the vibrational structure, that is still discernible at T = 300 K. This is in agreement with experiment in dioxane,[4] though the experimental spectrum appear less resolved than the computational counterpart. This might be due to inaccuracies in the simulation of the vibrational structure, as well as to an underestimation of the solvent inhomogeneous broadening, here simulated phenomenologically with a Gaussian with HWHM = 0.03 eV.

In agreement with experiment the absorption spectrum at T = 300 K is much broader than the emission one, and the vibrational structure of the (3N-7)D block is practically completely washed out by the ϕ spectrum. The same inaccuracies discussed above for emission probably explain the weak modulation (a reminiscence of the vibrational structure) in the computed absorption spectrum that is not seen in experiment.

To understand whether the drastically different broadening induced by the ϕ degree of freedom in absorption and emission at T = 300 K is a quantum phenomenon, i.e. if it requires a quantum description of the spectrum line shape $\sigma_\phi(\omega,T)$, we computed $\sigma_\phi(\omega,T)$ also according to the classical recipe described in Section 2.2. Figure 8 shows that the absorption and emission spectra at T = 300 K obtained computing $\sigma_\phi(\omega,300K)$ either at the quantum or at the classical level are extremely similar, indicating that classical approximation describes the broadening phenomenon quite satisfactorily. The good performance of the classical approximation is

dx.doi.org/10.1021/ct300664d | J. Chem. Theory Comput. 2012, 8, 4483−4493

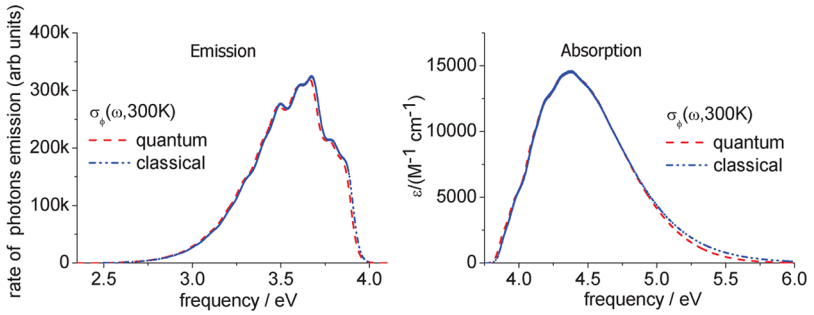

Figure 8. Comparison of the absorption and emission spectra of dithiophene at 300 K obtained computing the spectrum line shape due to the ϕ degree of freedom at the quantum level and according to a classical approximation.

discussed in the SI where the quantum and classical line shapes $\sigma_\phi(\omega,300K)$ for absorption an emission are compared, and the classical probability densities for torsion (only trans isomer is considered) on the ground ($P^0(\phi,300K)$) and excited state ($P^1(\phi,300K)$) are given. It is clearly seen that the quantum and classical $\sigma_\phi(\omega,300K)$ are very similar for absorption, while modest differences exist for emission, where however the broadening introduced by torsion is negligible. The inspection of $P^0(\phi,300K)$ and $P^1(\phi,300K)$ clearly indicates that the different broadening of absorption and emission arises from the fact that, due to the different shape and width, $P^0(\phi,300K)$ samples a much larger portion of $V^1(\phi)-V^0(\phi)$ than $P^1(\phi,300K)$ does. It is also remarkable that $P^1(\phi,300K)$ is extremely similar to the quantum Wigner distribution at 300 K obtained for an harmonic oscillator with $\omega \approx 85$ cm^{-1} and to the exact quantum distribution obtained numerically from the anharmonic S_1 ϕ states, further corroborating the fact that all the ϕ eigenstates on S_1 populated at room temperature are essentially harmonic. As a last comment it is worth noting that, clearly, the broadening induced by ϕ degree of freedom in the absorption spectrum at $T = 0$ K cannot be reproduced classically. Nonetheless, $V^1(\phi) - V^0(\phi)$ is so steep (and large, ≈ 0.12 eV) around the minimum of $V^0(\phi)$ ($\phi \approx 25°$ degrees) that even a classical distribution obtained with a fairly low temperature (few K degrees) is able to introduce a substantial broadening and a blue-shift in the absorption spectrum, as it happens at the quantum level (compare the shape and the maximum of the spectra in the top right and bottom right panels of Figure 7).

Due to the long progression exhibited by the ϕ spectrum even at very low temperature, the T2 spectra at $T = 1$ and 77 K are predicted to be broad and without remarkable vibrational structure, in contrast with what was observed in ethanol at 77 K. Since, as we discussed above, the extent of the predicted broadening in the computed spectra naturally arises from the double-well profile of the S_0 energy along ϕ, we are lead to conclude that such an energy profile is modified in ethanol at 77 K (melting point 159 K). In fact, due to the small energy differences of planar and nonplanar configurations in the gas phase, it is reasonable to assume that in the solvent matrix the planar configuration becomes favored with respect to the nonplanar one, since it occupies a smaller cavity. It is noteworthy that, assuming a planar S_0 geometry and assigning to ϕ an harmonic energy profile with a small real frequency, the thermal broadening of the spectrum at $T = 77$ K is strongly reduced, providing spectra in much better agreement with the experimental ones in ethanol at the same temperature. In Figure 9 we report the spectra obtained at $T = 77$ and 300 K assigning to $Q_1^{(0)}$ an harmonic frequency of $\approx$30 cm^{-1} obtained

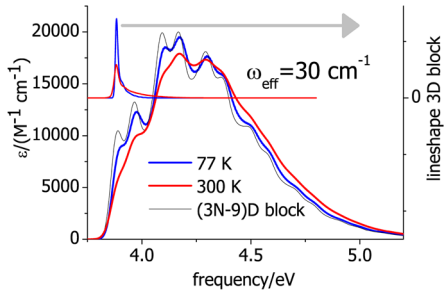

Figure 9. CAM-B3LYP/6-31G(d) absorption spectra for T2 at $T = 77$ (blue lines) and 300 K (red lines) assuming a planar minimum for S_0 and an harmonic profile along $Q_1^{(0)}$ with an effective frequency ω_{eff} = 30 cm^{-1}. The spectra have been computed block-diagonalizing the system in two blocks 3D (lowest-frequency modes) and (3N-9)D. Our calculations predict negligible temperature effects for the spectrum of the (3N-9)D block (black thin line). As explained in the text the spectra of the complete system can be considered convoluted with a Gaussian with HWHM = 0.03 eV.

by fitting the S_0 energy profile along ϕ in Figure 6 to a parabola (The SI shows the spectrum computed adopting the absolute value of the imaginary frequency along $Q_1^{(0)}$, i.e. 48 cm^{-1}). Even in this case we made use of block-diagonalization in order to speed up the calculations, and we set a very high threshold 1-ϵ = 0.99 (i.e., essentially block-diagonalization is exact) obtaining a 3D block encompassing the lowest-frequency three modes and a (3N-9)D block comprising the remaining modes. Notice that while the 77 K spectrum is in better agreement with experiment than what predicted accounting for the nonplanar minimum, the agreement with experiment at 300 K deteriorates, since the computed spectrum shows a marked residual vibrational structure (not very different from emission); the absorption maximum from $T = 77$ K (planar S_0) to $T = 300$ K (nonplanar S_0) is blue-shifted by $\approx$1700 cm^{-1}, a value close to the experimental shift, i.e. 1300 cm^{-1}.[5]

4. CONCLUDING REMARKS

In this paper we report the results of a thorough computational study of the absorption and emission spectra of dithiophene in different environments, from the gas phase to polar solvents. The vibrational structure of this prototype molecule has been simulated at zero and finite temperature without resorting to any empirical procedure. We took into account changes in the vibrational modes associated with the electronic transition (Duschinsky effect), increasing the accuracy of the computed spectra. Indeed, the relative intensity and the position of the high resolution emission spectrum are very well reproduced, and, when using a fairly large basis set and considering

anharmonic corrections, the agreement between experimental and computed spectra is almost quantitative (the average deviation for the 8 lowest energy main peaks is ∼13 cm^{-1}, CAM-B3LYP/6-311+G(2d,2p) calculations). While for the emission spectrum inclusion of the Duschinsky effect 'simply' leads to a more accurate determination of the relative intensity of the different peaks, it is necessary for a proper assignment of the absorption spectrum. We indeed show the Dushinsky mixings induces a splitting of some absorption stick bands reproducing experimental features not understandable with simpler models (like Adiabatic Shift, AS) that neglect them. The remarkable effect of the temperature on the spectra has also been reproduced, by using a nonempirical procedure and properly treating the vibrational states associated with the ϕ torsion. Confirming previous suggestions, such an effect depends on the fact that the potential energy surfaces associated with the torsional inter-ring molecular modes are much more shallow in the ground electronic state than in the excited state. On the other hand, while in the gas phase the molecule is not planar, and the PES associated with the lowest frequency torsional modes exhibit a double well, separated by a very small barrier that nonetheless support localized states, our calculations suggest that the molecule, when embedded in a glass matrix, is planar also in the ground state. Indeed, including the effect of the double well at the anharmonic level leads to broad and unresolved spectra also at 1 K, in disagreement with the experimental results.

All the density functionals we have tested provide a good qualitative description of the absorption and emission spectra, but CAMB3LYP and PBE0 are the most accurate. In particular, the spectra computed at the SS-PCM/CAM-B3LYP/6-311+G-(2d,2p) level in solution are practically superposable to the experimental ones. PCM/TD-DFT calculations allow for an accurate evaluation of Stokes shift in solution, though solvent effect is somewhat underestimated. An accurate evaluation of solvent effect on a transition involving a very modest shift of the electron density, especially in a nonpolar environment, requires indeed a quantum mechanical treatment of dispersive interactions,[69] as those depending on the polarizability of the solute and of the solvent molecules, which are not considered in standard PCM calculations.[69]

Overall the results here reported confirm that it is possible to obtain spectra directly comparable and in very good agreement with the experiment without resorting to any empirical parameter or ad-hoc scaling procedure,[65] providing encouraging indications on the usefulness of fully ab initio approaches for the study of vibronic interactions in material science.

In this respect, the availability of fairly resolved spectra also in supramolecular complexes[13] of technological interest increases the usefulness of a procedure able to provide accurate assignment of the vibrational features and to dissect all the chemical physical factors (intra- and intermolecular interactions, solvent, temperature) influencing the shape of absorption and emission spectra.

■ ASSOCIATED CONTENT

Supporting Information

Schematic description of the most relevant vibrational modes of T2. Additional information on the comparison between the different functionals and analysis of the basis set effect. Further details on our treatment of the lowest energy torsional mode. This material is available free of charge via the Internet at http://pubs.acs.org.

■ AUTHOR INFORMATION

Corresponding Author

*E-mail: fabrizio.santoro@iccom.cnr.it (F.S.), robimp@unina.it (R.I.).

Notes

The authors declare no competing financial interest.

■ ACKNOWLEDGMENTS

The authors thank the Italian Institute of Technology (project IIT-Seed HELYOS) and MIUR (PRIN 2008 "TIME", PRIN 2008 "Architetture ibride multifunzionali basate su biomolecole per applicazioni nel campo della sensoristica, della conversione di energia e del biomedicale", FIRB 'Futuro in Ricerca RBFR08DUX6-003 and RBFR10Y5VW) for financial support.

■ REFERENCES

(1) (a) Garnier, F.; Hajlaoui, R.; Yassar, A.; Srivastava, P. *Science* **1994**, *265*, 1684−1686. (b) Garnier, F.; Hajlaoui, R.; El Kassmi, A.; Horowitz, G.; Laigre, L.; Porzio, W.; Armanini, M.; Provasoli, F. *Chem. Mater.* **1998**, *10*, 3334−3339. (c) Friend, S. H.; Gymer, R. W.; Holmes, A. B.; Burroughes, J. H.; Marks, R. N.; Taliani, C.; Bradley, D. D. C.; Dos Santos, D. A.; Brédas, J. L.; Lögdlund, M.; Salaneck, W. R. *Nature* **1999**, *397*, 121−128. (d) Dimitrakopoulos, C. D.; Malenfant, P. R. L. *Adv. Mater.* **2002**, *14*, 99−117. (e) Fichou, D. *Handbook of Oligo- and Polythiophenes*; Wiley-VCH: Weinheim, 1999. (f) Facchetti, A.; Yoon, M.-H.; Stern, C. L.; Hutchinson, G. R.; Ratner, M. A.; Marks, T. J. *J. Am. Chem. Soc.* **2004**, *126*, 13480−13501. (g) Yoon, M.-H.; DiBenedetto, S. A.; Russell, M. T.; Facchetti, A.; Marks, T. J. *Chem. Mater.* **2007**, *19*, 4864−4881. (h) Murphy, A. R.; Fréchet, J. M. J. *Chem. Rev.* **2007**, *107*, 1066−1096. (i) *Handbook of Thiophene-Based Materials: Applications in Organic Electronics and Photonics*; Perepichka, I. F., Perepichka, D. F., Eds.; John Wiley & Sons: Chichester, 2009.

(2) Zade, S. S.; Zamoshchik, N.; Bendikov, M. *Acc. Chem. Res.* **2011**, *44*, 14−24.

(3) Gierschner, J.; Cornil, J.; Egelhaaf, H.-J. *Adv. Mater.* **2007**, *19*, 173−191.

(4) Becker, R. S.; de Melo, J. S.; Maçanita, A. L.; Elisei, F. *J. Phys. Chem.* **1996**, *100*, 18683−18695.

(5) Becker, R. S.; de Melo, J. S.; Maçanita, A. L.; Elisei, F. *Pure Appl. Chem.* **1995**, *67*, 9−16.

(6) Takayanagi, M.; Gejo, T.; Hanazaki, I. *J. Phys. Chem.* **1994**, *98*, 12893−12898.

(7) Belletete, M.; Leclerc, M.; Durocher, G. *J. Phys. Chem.* **1994**, *98*, 9450−9456.

(8) Yang, A.; Kuroda, M.; Shiraishi, Y.; Kobayashi, T. *J. Phys. Chem. B* **1998**, *102*, 3706−3711.

(9) Chadwick, J. E.; Kohler, B. E. *J. Phys. Chem.* **1994**, *98*, 3631−3637.

(10) Birnbaum, D.; Kohler, B. E. *J. Chem. Phys.* **1989**, *90*, 3506−3510.

(11) Birnbaum, D.; Fichou, D.; Kohler, B. E. *J. Chem. Phys.* **1992**, *96*, 165−169.

(12) Birnbaum, D.; Kohler, B. E. *J. Chem. Phys.* **1991**, *95*, 4783−4789.

(13) Gao, J.; Blondeau, P.; Salice, P.; Menna, E.; Bártová, B.; Hébert, C.; Leschner, J.; Kaiser, U.; Milko, M.; Ambrosch-Draxl, C.; Loi, M. A. *Small* **2011**, *7*, 1721−1721.

(14) Aragó, J.; Viruela, P. M.; Gierschner, J.; Ortí, E.; Milián Medina, B. *Phys. Chem. Chem. Phys.* **2011**, *13*, 1457−1465.

(15) Macchi, G.; Milián Medina, B.; Zambianchi, M.; Tubino, R.; Cornil, J.; Barbarella, G.; Gierschner, J.; Meinardi, F. *Phys. Chem. Chem. Phys.* **2009**, *11*, 984−990.

(16) Milián Medina, B.; Wasserberg, D.; Meskers, S. C. J.; Mena-Osteritz, E.; Bäuerle, P.; Gierschner, J. *J. Phys. Chem. A* **2008**, *112*, 13282−13286.

(17) Milián Medina, B.; Van Vooren, A.; Brocorens, P.; Gierschner, J.; Shkunov, M.; Heeney, M.; McCulloch, I.; Lazzaroni, R.; Cornil, J. *Chem. Mater.* **2007**, *19*, 4949−4956.
(18) Gierschner, J.; Mack, H.-G.; Egelhaaf, H.-J.; Schweizer, S.; Doser, B.; Oelkrug, D. *Synth. Met.* **2003**, *138*, 311−315.
(19) Petelenz, P.; Andrzejak, M. *J. Chem. Phys.* **2000**, *113*, 11306−11314.
(20) Zhao, Z.; Spano, F. C. *J. Chem. Phys.* **2005**, *122*, 114701−114711.
(21) Spano, F. C.; Silvestri, L.; Spearman, P.; Raimondo, L.; Tavazzi, S. *J. Chem. Phys.* **2007**, *127*, 184703−184714.
(22) Andrzejak, M.; Pawlikowski, M. T. *J. Phys. Chem. A* **2008**, *112*, 13737−13744.
(23) Vujanovich, E. C.; Bloom, J. W. G.; Wheeler, S. E. *J. Phys. Chem. A* **2012**, *116*, 2997−3003.
(24) Negri, F.; Zgierski, M. Z. *J. Chem. Phys.* **1994**, *100*, 2571−2587.
(25) Heimel, G.; Daghofer, M.; Gierschner, J.; List, E. J. W.; Grimsdale, A. C.; Müllen, K.; Beljonne, D.; Brédas, J.-L.; Zojer, E. *J. Chem. Phys.* **2005**, *122*, 54501−54511.
(26) (a) Furche, F.; Ahlrichs, R. *J. Chem. Phys.* **2002**, *117*, 7433. (b) Caillie, C. V.; Amos, R. D. *Chem. Phys. Lett.* **1999**, *308*, 249;(c) *ibidem* **2000**, *317*, 159.
(27) Becke, A. D. *Phys. Rev. A* **1988**, *38*, 3098−3100.
(28) Lee, C.; Yang, W.; Parr, R. G. *Phys. Rev. B* **1988**, *37*, 785−789.
(29) Becke, A. D. *J. Chem. Phys.* **1993**, *98*, 5648−5652.
(30) Adamo, C.; Barone, V. *J. Chem. Phys.* **1999**, *110*, 6158−6169.
(31) Becke, A. D. *J. Chem. Phys.* **1993**, *98*, 1372−1377.
(32) Yanai, T.; Tew, D.; Handy, N. *Chem. Phys. Lett.* **2004**, *393*, 51−57.
(33) Tomasi, J.; Mennucci, B.; Cammi, R. *Chem. Rev.* **2005**, *105*, 2999−3093.
(34) Cossi, M.; Barone, V. *J. Chem. Phys.* **2001**, *115*, 4708−4717.
(35) Scalmani, G.; Frisch, M. J.; Mennucci, B.; Tomasi, J.; Cammi, R.; Barone, V. *J. Chem. Phys.* **2006**, *124*, 94107−94121.
(36) Improta, R.; Barone, V.; Scalmani, G.; Frisch, M. J. *J. Chem. Phys.* **2006**, *125*, 54103−54111.
(37) Improta, R.; Frisch, M. J.; Scalmani, G.; Barone, V. *J. Chem. Phys.* **2007**, *127*, 74504−74512.
(38) (a) Improta, R. UV-Visible Absorption and Emission Energies in Condensed phase by PCM-TD-DFT methods. In *Computational Strategies for Spectroscopy: from Small Molecules to Nanosystems*; Barone, V., Ed.; John Wiley & Sons: Chichester, 2011; pp 39−76.
(39) Frisch, M. J.; Trucks, G. W.; Schlegel, H. B.; Scuseria, G. E.; Robb, M. A.; Cheeseman, J. R.; Scalmani, G.; Barone, V.; Mennucci, B.; Petersson, G. A.; Nakatsuji, H.; Caricato, M.; Li, X.; Hratchian, H. P.; Izmaylov, A. F.; Bloino, J.; Zheng, G.; Sonnenberg, J. L.; Hada, M.; Ehara, M.; Toyota, K.; Fukuda, R.; Hasegawa, J.; Ishida, M.; Nakajima, T.; Honda, Y.; Kitao, O.; Nakai, H.; Vreven, T.; Montgomery, J. A., Jr.; Peralta, J. E.; Ogliaro, F.; Bearpark, M.; Heyd, J. J.; Brothers, E.; Kudin, K. N.; Staroverov, V. N.; Kobayashi, R.; Normand, J.; Raghavachari, K.; Rendell, A.; Burant, J. C.; Iyengar, S. S.; Tomasi, J.; Cossi, M.; Rega, N.; Millam, J. M.; Klene, M.; Knox, J. E.; Cross, J. B.; Bakken, V.; Adamo, C.; Jaramillo, J.; Gomperts, R.; Stratmann, R. E.; Yazyev, O.; Austin, A. J.; Cammi, R.; Pomelli, C.; Ochterski, J. W.; Martin, R. L.; Morokuma, K.; Zakrzewski, V. G.; Voth, G. A.; Salvador, P.; Dannenberg, J. J.; Dapprich, S.; Daniels, A. D.; Farkas, Ö.; Foresman, J. B.; Ortiz, J. V.; Cioslowski, J.; Fox, D. J. *Gaussian 09, Revision A.2*; Gaussian, Inc.: Wallingford, CT, 2009.
(40) (a) Biczysko, M.; Bloino, J.; Santoro, F.; Barone, V. Time-Independent Approaches to Simulate Electronic Spectra Lineshapes: From Small Molecules to Macrosystems. In *Computational Strategies for Spectroscopy: from Small Molecules to Nanosystems*; Barone, V., Ed.; John Wiley & Sons: Chichester, 2011; pp 361−443. (b) Lami, A.; Santoro, F. Time-Dependent Approaches to Calculation of Steady-State Vibronic Spectra: From Fully Quantum to Classical Approaches. In *Computational Strategies for Spectroscopy: from Small Molecules to Nano Systems*; Barone, V., Ed.; John Wiley & Sons: Chichester, 2011; pp 475−516.
(41) Avila Ferrer, F. J.; Santoro, F. *Phys. Chem. Chem. Phys* **2012**, *14*, 13549−13560.
(42) (a) Hazra, A.; Noiijen, M. *J. Chem. Phys.* **2005**, *122*, 204327. (b) Hazra, A.; Noiijen, M. *Phys. Chem. Chem. Phys.* **2005**, *7*, 1759.
(43) Santoro, F.; Lami, A.; Improta, R.; Barone, V. *J. Chem. Phys.* **2007**, *126*, 184102−184112.
(44) Bloino, J.; Biczysko, M.; Santoro, F.; Barone, V. *J. Chem. Theory Comput.* **2010**, *6*, 1256−1274.
(45) Kupka, H.; Cribb, P. H. *J. Chem. Phys.* **1986**, *85*, 1303−1315.
(46) Peluso, A.; Santoro, F.; Del Re, G. *Int. J. Quantum Chem.* **1997**, *63*, 233−244.
(47) Santoro, F.; Improta, R.; Lami, A.; Bloino, J.; Barone, V. *J. Chem. Phys.* **2007**, *126*, 84509−84521; *Ibid.* **2007**, *126*, 169903−169903.
(48) Santoro, F.; Improta, R.; Lami, A.; Bloino, J.; Barone, V. *J. Chem. Phys.* **2008**, *128*, 224311−224327.
(49) Santoro, F.; Barone, V. *Int. J. Quantum Chem.* **2010**, *110*, 476−486.
(50) Barone, V.; Bloino, J.; Biczysko, M.; Santoro, F. *J. Chem. Theory Comput.* **2009**, *5*, 540−554.
(51) Picconi, D.; Lami, A.; Santoro, F. *J. Chem. Phys.* **2012**, *136*, 244104−244121.
(52) Improta, R.; Barone, V.; Santoro, F. *Angew. Chem., Int. Ed.* **2007**, *46*, 405−408.
(53) Improta, R.; Barone, V.; Santoro, F. *J. Phys. Chem. B* **2007**, *111*, 14080−14082.
(54) Santoro, F.; , *FCclasses* a Fortran 77 code. Available at http://village.pi.iccom.cnr.it/Software (accessed October 15, 2012).
(55) Beenken, W. J. D. *Chem. Phys.* **2008**, *349*, 250−255.
(56) Borrelli, R.; Peluso, A. *J. Chem. Phys.* **2006**, *125*, 194308−194315.
(57) Borrelli, R.; Peluso, A. *J. Chem. Phys.* **2006**, *128*, 44303−44309.
(58) Andrzejak, M.; Witek, H. A. *Theor. Chem. Acc.* **2011**, *129*, 161−172.
(59) Siegrist, T.; Kloc, C.; Laudise, R. A.; Katz, H. E.; Haddon, R. C. *Adv. Mater.* **1998**, *10*, 379−382.
(60) Dierksen, M.; Grimme, S. *J. Phys. Chem. A* **2004**, *108*, 10225−10237.
(61) Jacquemin, D.; Perpete, E. A.; Ciofini, I.; Adamo, C. *Acc. Chem. Res.* **2009**, *42*, 326−334.
(62) Jacquemin, D.; Planchat, A.; Adamo, C.; Mennucci, B. *J. Chem. Theory Comput.* **2012**, *8*, 2359−2372.
(63) Jacquemin, D.; Brémond, E.; Planchat, A.; Ciofini, I.; Adamo, C. *J. Chem. Theory Comput.* **2011**, *7*, 1882−1892.
(64) Lopez, G. V.; Chang, C.-H.; Johnson, P. M.; Hall, G. E.; Sears, T. J.; Markiewicz, B.; Milan, M.; Teslja, A. *J. Phys. Chem. A* **2012**, *116*, 6750−6758.
(65) Avila Ferrer, F. J.; Improta, R.; Santoro, F.; Barone, V. *Phys. Chem. Chem. Phys.* **2011**, *13*, 17007−17012.
(66) Lewis, J. D.; Malloy, T. B.; Chao, T. H.; Laane, J. *J. Mol. Struct.* **1972**, *12*, 427−449.
(67) (a) Cammi, R.; Corni, S.; Mennucci, B.; Tomasi, J. *J. Chem. Phys.* **2005**, *122*, 104513−104524. (b) Corni, S.; Cammi, R.; Mennucci, B.; Tomasi, J. *J. Chem. Phys.* **2005**, *123*, 134512−134521.
(68) McRae, E. G. *J. Phys. Chem.* **1957**, *61*, 562−572.
(69) (a) Weijo, V.; Mennucci, B.; Frediani, L. *J. Chem. Theory Comput.* **2010**, *6*, 3358−3364. (b) Amovilli, C.; Mennucci, B. *J. Phys. Chem. B* **1997**, *101*, 1051−1057. (c) Curutchet, C.; Orozco, M.; Luque, F. J.; Mennucci, B.; Tomasi, J. *J. Comput. Chem.* **2006**, *27*, 1769−1780.
(70) Barone, V. *J. Chem. Phys.* **2005**, *122*, 014108.